Near-Field Channel Estimation via Deep Unfolding for Extremely Large-scale Antenna Arrays

Nguyen The Khang[1], Do Hai Son[12], Tran Trong Duy[13], Trung Thanh Le[1],
Viet-Dung Nguyen[4], Trong-Minh Hoang[5], Karim Abed-Meraim[6], Merouane Debbah[7], and Nguyen Linh Trung[1*]
[1] VNU University of Engineering and Technology, Vietnam National University, Hanoi, Vietnam
[2] School of Electrical Engineering, Computing and Mathematical Sciences, Curtin University, Australia
[3] CentraleSupélec, Université Paris-Saclay, CNRS, L2S, Gif-sur-Yvette, France
[4] Spectrum Engineering Department, French Spectrum Management Agency, Brest, France
[5] Posts and Telecommunications Institute of Technology, Hanoi, Vietnam
[6] PRISME Laboratory (IUF member), University of Orléans, Orléans, France
[7] Khalifa University, Abu Dhabi, United Arab Emirates

***Abstract*—The Extremely Large-scale Antenna Array (ELAA) has been envisioned as a promising candidate to meet the ambitious demands of 6G. However, this evolution also brings about two primary limitations: high computational complexity caused by large-scale arrays and inherent operation in the near-field region. To address these issues, this work exploits the sparsity of near-field channels in the polar domain and formulates channel estimation as a compressed sensing (CS) problem, thereby enabling estimation with reduced pilot overhead. In particular, we propose a guideline to design a sparsifying codebook for the near-field channel, which is strictly based on a target coherence value. Building on this, we develop a deep unfolding architecture, derived from the iterative solver ISTA, with a hybrid loss, namely Hybrid LISTA. Numerical results demonstrate that our proposed codebook, with comparable complexity, still exhibits improved estimation performance and greater coverage in the near-field region. Moreover, our unfolded model with the hybrid loss consistently delivers better recovery performance over existing estimation schemes.**

***Index Terms*—Extremely large-scale antenna array, near-field channel estimation, compressed sensing, deep unfolding.**

I. INTRODUCTION

Arising from the ambitious performance targets of transformative 6G applications, extremely large-scale antenna arrays (ELAAs) and higher-frequency technologies are key enablers, promising ten-fold spectral efficiency gains, 1 Tbps peak rates, and seamless coverage [1]. Leveraging multi-antenna techniques that enhance spectral efficiency and spatial resolution, the core concept of ELAA is to deploy hundreds or thousands of antennas in a compact aperture area [2]. Despite these promising prospects, their integration introduces two main obstacles for channel estimation. First, high-dimensional channel matrices introduce extreme baseband complexity [1]. To mitigate this, the BS adopts a hybrid precoding architecture with reduced RF-chain blocks, which in turn increases pilot overhead to obtain accurate channel state information. Second, the usage of ELAA and operations in higher-frequency band push communication systems into the near-field (NF) region, where spherical wavefronts characterize the channel phase as a function of both angle and distance [1]. This expands the parameter search space and further increases pilot overhead and computation complexity.

CS is a technique designed to recover high-dimensional sparse signals from a limited number of measurements [3]. With the usage of ELAA, the NF channel exhibits sparsity in the polar domain (i.e., angle and distance), enabling accurate channel estimation based on CS with reduced pilot overhead. The authors of [4] proposed a polar-domain codebook design for NF channel. However, their resulting coherence remains considerably high, which implies strong column correlation that leads to an ill-conditioned CS problem. Moreover, their codebook construction relied on a grid search for a suitable choice of codebook parameter, lacking a direct link to codebook coherence. Another codebook proposed in [5] achieved perfectly independent columns by coupling distance and angle parameters. However, that codebook must be adaptively refined based on user locations, incurring high computational overhead for its dynamic updates. Deep Unfolding is a branch of model-based deep learning, which converts an iterative algorithm into a deep neural network by designing each layer to resemble a single iteration [6]. The original concept was proposed in [7], introducing the unfolding architecture of iterative soft thresholding algorithm (ISTA) for sparse recovery. The works in [8], [9] proposed to apply the unfolded Learned ISTA (LISTA) models for NF channel estimation problems. However, their loss functions typically rely on the sparse representation of NF channels, which may lead to avoidable performance degradation due to their ill-conditioned sparsifying codebooks.

Although the strict coherence condition required for CS problems must be kept quite low [3], this consequently limits the coverage of the codebook grid, as grid points must be sampled sparsely to maintain low coherence [4]. This constraint is typically too restrictive in practice, especially when our objective is to estimate the channel indirectly via CS, rather than to recover a perfectly unique sparse solution. As argued in [3], this condition can be relaxed to be kept at a reasonably

*This research was funded by the research project QG.25.08 of Vietnam National University, Hanoi. Correspondence: Nguyen Linh Trung (linhtrung@vnu.edu.vn).

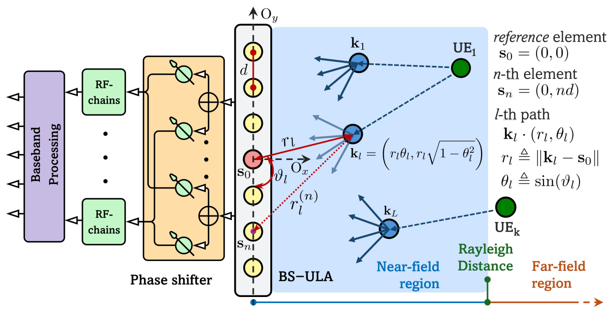

Fig. 1. System layout of the uplink channel estimation.

low level to facilitate efficient grid sampling. Based on these insights, the main contributions in this work can be outlined as follows

- We propose a polar-domain codebook design for NF channel. The framework establishes an explicit mapping from a target coherence to the codebook parameter, enabling direct construction based on a desired coherence.
- We develop a Hybrid LISTA (H-LISTA) network for NF channel estimation in ELAA systems serving multiple single-antenna users. Leveraging the proposed codebook, we introduce a hybrid loss function that accounts for both the sparse representation and the reconstructed channel simultaneously.
- We provide extensive numerical results demonstrating the effectiveness of the proposed codebook and H-LISTA model. With a comparable number of grid points, our codebook achieves superior recovery performance over existing designs across various SNR cases. Moreover, the H-LISTA model consistently outperforms other unfolded networks and conventional estimation methods while using fewer layers.

II. Problem Formulation

We consider an uplink channel estimation of ELAA system serving multiple single-antenna users. The base station (BS) is equipped with a uniform linear array (ULA) of $N = 2N_r + 1$ antennas with half-wavelength spacing $d = \lambda_c/2$. As depicted in Fig. 1, the array is placed along the y-axis with its center element $\mathbf{s}_0$ at the origin, the n-th element is located at $\mathbf{s}_n = (0, nd)$, where $n = -N_r, \ldots, N_r$. To reduce hardware cost and power consumption, the BS employs a hybrid analog-digital precoding architecture with N_{RF} RF-chains, where $N_{\mathrm{RF}} \ll N$. Assume that K users transmit mutually orthogonal pilot sequences, so that channel estimation for each user can be performed independently. Without loss of generality, we consider the channel of an arbitrary user $\mathbf{h} \in \mathbb{C}^{N\times 1}$.

A. System Model

For simplicity, the pilot symbol at time slot p is set as $x_p = 1$ for all $p = 1, \ldots, P$ (P being the pilot sequence length). The corresponding received signal at the BS denoted by $\mathbf{y}_p \in \mathbb{C}^{N_{\mathrm{RF}}\times 1}$ is formulated as

$$\mathbf{y}_p = \mathbf{A}_p \mathbf{h} + \mathbf{n}_p, \tag{1}$$

where analog combiner matrix $\mathbf{A}_p \in \mathbb{R}^{N_{\mathrm{RF}}\times N}$ is implemented by phase shifters, satisfying $[\mathbf{A}_p]_{i,j} = 1/\sqrt{N}$, and $\mathbf{n}_p \sim \mathcal{CN}(\mathbf{0}, \sigma^2 \mathbf{A}_p \mathbf{A}_p^\top)$ denotes the effective noise. After observing P time slots, the overall received sequence is vertically concatenated as $\mathbf{y} = [\mathbf{y}_1^\top, \cdots, \mathbf{y}_P^\top]^\top \in \mathbb{C}^{P\cdot N_{\mathrm{RF}}\times 1}$,

$$\mathbf{y} = \mathbf{A}\mathbf{h} + \mathbf{n}, \tag{2}$$

where $\mathbf{A} = [\mathbf{A}_1^\top, \cdots, \mathbf{A}_P^\top]^\top \in \mathbb{R}^{P\cdot N_{\mathrm{RF}}\times N}$ is the overall combining matrix with its wide shape (i.e., $P \cdot N_{\mathrm{RF}} < N$), and $\mathbf{n} = [\mathbf{n}_1^\top, \cdots, \mathbf{n}_P^\top]^\top \in \mathbb{C}^{P\cdot N_{\mathrm{RF}}\times 1}$ is overall noise. For a vector $\mathbf{v}$, its corresponding transpose and conjugate transpose vectors can be denoted as $\mathbf{v}^\top$ and $\mathbf{v}^{\mathrm{H}}$, respectively.

B. Channel Model

Considering a rich-scattering environment, we assume L scatterers in the NF region, each contributing to a path, described by $\mathbf{k}_l$ with angle θ_l and distance r_l. The channel is composed by L multi-path components as in [1], [10]

$$\mathbf{h} = \sqrt{\frac{N}{L}} \sum_{l=1}^{L} g_l \exp(-j\tfrac{2\pi}{\lambda_c} r_l)\, \mathbf{a}(\theta_l, r_l), \tag{3}$$

where g_l is the channel gain and the array response vector $\mathbf{a}(\theta_l, r_l) \in \mathbb{C}^{N\times 1}$ is normalized to the unit norm (i.e., $\|\mathbf{a}\|_2 = 1$), and its n-th entry reflects the phase shift from $\mathbf{s}_n$ to $\mathbf{s}_0$,

$$\mathbf{a}(\theta_l, r_l) = \frac{1}{\sqrt{N}} \left[\cdots, \exp\left[-j\tfrac{2\pi}{\lambda_c}(r_l^{(n)} - r_l)\right], \cdots\right]^\top. \tag{4}$$

In NF region, the distance from $\mathbf{k}_l$ to $\mathbf{s}_n$ is denoted by $r_l^{(n)}$, which can be approximated by the second-order Taylor expansion as

$$r_l^{(n)} \approx r_l - nd\theta_l + \frac{n^2 d^2 (1-\theta_l^2)}{2r_l}. \tag{5}$$

Leveraging NF beamfocusing, the NF channel can exhibit sparsity through a codebook in the polar domain. The intuition behind this codebook is to create a discretized grid alternating the continuous search space of channel parameters (θ_l, r_l). Particularly, the NF channel can be expressed sparsely as

$$\mathbf{h} \approx \mathbf{W}\boldsymbol{\alpha}, \quad \text{s.t.,} \quad \|\boldsymbol{\alpha}\|_0 \ll G, \tag{6}$$

where the codebook is $\mathbf{W} \in \mathbb{C}^{N\times G}$, consisting of G points and its sparse representation $\boldsymbol{\alpha} \in \mathbb{C}^{G\times 1}$. With each point is parameterized by $(\hat{\theta}_i, \hat{r}_{i,s})$, that codebook is constructed as

$$\begin{aligned}\mathbf{W} = \Big[&\mathbf{a}(\hat{\theta}_1, \hat{r}_{1,1}), \cdots, \mathbf{a}(\hat{\theta}_1, \hat{r}_{1,S_1}), \cdots, \\ &\cdots, \mathbf{a}(\hat{\theta}_i, \hat{r}_{i,s}), \cdots, \mathbf{a}(\hat{\theta}_I, \hat{r}_{I,1}), \cdots, \mathbf{a}(\hat{\theta}_I, \hat{r}_{I,S_I})\Big],\end{aligned} \tag{7}$$

with I angular rays and S_i points along i-th ray. The low coherence is desirable for CS as it brings the codebook closer to the unitarity property which favors the uniqueness of $\boldsymbol{\alpha}$ [11] (i.e., $\mathbf{W}^{\mathrm{H}}\mathbf{W} \approx \mathbf{I}_G$). For two arbitrary columns $\mathbf{a}_p$ and $\mathbf{a}_q$ of $\mathbf{W}$, the mutual coherence is formally expressed as

$$\begin{aligned}\mu(\mathbf{W}) &= \max_{p\neq q} \frac{|\mathbf{a}_p^{\mathrm{H}}\mathbf{a}_q|}{\|\mathbf{a}_p\|_2 \|\mathbf{a}_q\|_2} = \max_{p\neq q} |\mathbf{a}_p^{\mathrm{H}}\mathbf{a}_q|, \quad \mu \in [0,1] \\ &= \max_{p\neq q} \left| \tfrac{1}{N} \sum_{n=-N_r}^{N_r} \exp\left[-jn\pi\Delta_\theta + j\pi n^2 d \Delta_R(\hat{\theta}_p, \hat{\theta}_q)\right] \right|,\end{aligned} \tag{8}$$

where $\Delta_\theta = \hat{\theta}_p - \hat{\theta}_q$ and $\Delta_R(\hat{\theta}_p, \hat{\theta}_q) = \frac{1-\hat{\theta}_p^2}{2\hat{r}_p} - \frac{1-\hat{\theta}_q^2}{2\hat{r}_q}$ correspond to angular step and distance difference parameterized by angles, respectively.

The guideline in [4] constructs the codebook grid by forming several distance rings. Within the same ring (i.e., constrained by the condition $\frac{1-\hat{\theta}^2}{2\hat{r}} = \text{const}$, then $\Delta_R = 0$), the resulting coherence depends only on the angular step Δ_θ. The angles are sampled uniformly with $\Delta_\theta = 2/N$, thereby exhibiting intra-ring orthogonality. Consequently, the overall codebook coherence is primarily determined by inter-ring coherence, where β directly controls the grid granularity by ring sampling plan and the resulting codebook coherence. The concepts of intra-ring and inter-ring coherence will be discussed thoroughly in a later section.

C. Channel Estimation by Compressed Sensing

Through this alternating approach, the channel is estimated indirectly via its sparse-domain representation. The estimation can be formulated as the following optimization problem:

$$\min_{\boldsymbol{\alpha}} \|\boldsymbol{\alpha}\|_0 \quad \text{s.t.,} \quad \|\mathbf{y} - \boldsymbol{\Psi}\boldsymbol{\alpha}\|_2^2 \leq \epsilon, \tag{P_0}$$

where $\boldsymbol{\Psi} = \mathbf{A}\mathbf{W} \in \mathbb{C}^{P \cdot N_{\mathrm{RF}} \times G}$ denotes for the measurement matrix and ϵ corresponds to the acceptable estimation error. By relaxing the ℓ_0-norm in (P_0), the alternative objective function is obtained by embedding the constraints into a unified optimization objective function (P_1) as

$$\min_{\boldsymbol{\alpha}} \tfrac{1}{2}\|\mathbf{y} - \boldsymbol{\Psi}\boldsymbol{\alpha}\|_2^2 + \lambda\|\boldsymbol{\alpha}\|_1, \tag{P_1}$$

where $\lambda \in (0,1)$ is the Lagrange multiplier for balancing the estimation error and the sparsity of $\boldsymbol{\alpha}$. To solve the composite objective in (P_1), the proximal gradient descent (PGD) method for the ℓ_1-norm is ISTA [12], whose update rule is given by

$$[\boldsymbol{\alpha}]^k \triangleq \mathcal{S}_{\eta\lambda}\left\{(\eta\boldsymbol{\Psi}^{\mathrm{H}})\mathbf{y} + \left(\mathbf{I}_G - \eta\boldsymbol{\Psi}^{\mathrm{H}}\boldsymbol{\Psi}\right)[\boldsymbol{\alpha}]^{k-1}\right\}, \tag{9}$$

where $[\boldsymbol{\alpha}]^k$ is the solution at k-th iteration, the fixed step size $\eta = \Lambda_{\max}^{-1}$ is typically chosen as the inverse of the largest eigenvalue of $\boldsymbol{\Psi}^{\mathrm{H}}\boldsymbol{\Psi}$ for its convergence guarantee, and $\mathcal{S}_\theta\{z\} = \frac{z}{|z|}\max(0, |z| - \theta)$ corresponds to the soft-shrinkage function for promoting the sparsity of $\boldsymbol{\alpha}$.

III. Proposed Methods

In this section, we present our proposed framework for NF channel estimation, consisting of two key components. First, we design a polar-domain codebook directly controlled by mutual coherence. Second, we develop a deep unfolding network H-LISTA with a hybrid loss that accounts for both the sparse representation and the reconstructed channel.

A. Codebook Design

Our codebook design follows the ring-based structure of [4], but with two key modifications that allow direct control of coherence without a grid search for the parameter β. First, we employ the outermost ring by the effective Rayleigh distance (ERD) [13], which may effectively handle FF paths. Second, we adopt a denser angular sampling (i.e., a smaller step Δ_θ), which breaks the inherent orthogonality and introduces a non-zero intra-ring coherence μ_θ. This value then serves as a design target: we constrain the inter-ring coherence μ_β to approximately match μ_θ.

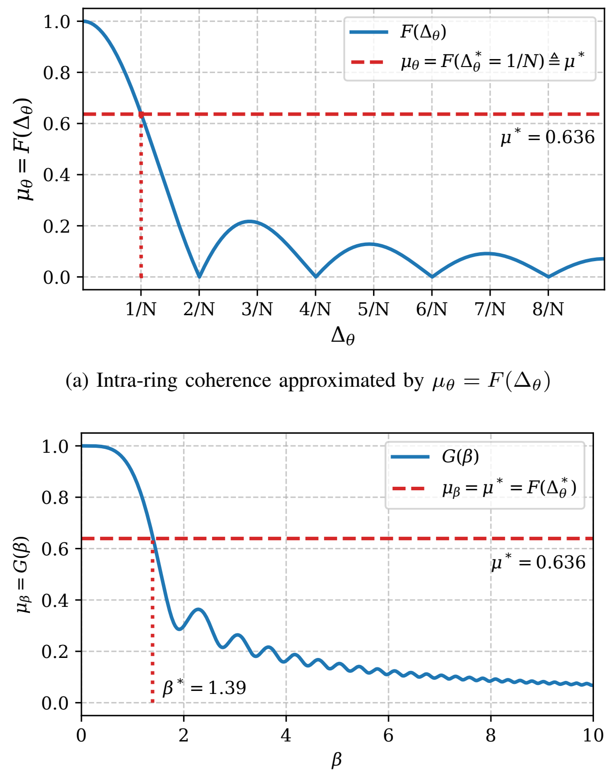

(a) Intra-ring coherence approximated by $\mu_\theta = F(\Delta_\theta)$

(b) Inter-ring coherence approximated by $\mu_\beta = G(\beta)$

Fig. 2. Intra-ring and inter-ring coherence functions.

1) Angular sampling: We adopt a denser angular sampling with $I \triangleq \zeta \cdot N, \zeta \geq 1$, whereas the codebook in [4] corresponds to $\zeta = 1$. The angular rays are uniformly sampled as

$$\hat{\theta}_i = \frac{2i - I - 1}{I}, \quad i = 1, \cdots, I, \tag{10}$$

so the angular step is $\Delta_\theta = 2/I$. Based on (8), the intra-ring coherence of two points lying on the same ring (i.e., $\Delta_R = 0$) can be computed as

$$\mu(\mathbf{W}) \approx \mu_\theta = F(\Delta_\theta) \triangleq \left|\frac{\sin(N\pi\Delta_\theta/2)}{N\sin(\pi\Delta_\theta/2)}\right|. \tag{11}$$

As shown in Fig. 2a, when the step Δ_θ increases, the corresponding coherence factor relatively decreases, which implies that the nearby points produce higher coherence values. Moreover, the zero-crossing points of $F(\Delta_\theta)$ match exactly with the proposed angular step in [4], thereby exhibiting their orthogonality among intra-ring points (i.e., $F(\Delta_\theta = \frac{2m}{N}) = 0, \forall m \neq 0$).

In this work, we upsample the angular grid by setting $\zeta = 2$, hence $\Delta_\theta^* = 1/N$, the resulting intra-ring coherence shifts to a non-zero $F(\Delta_\theta^* = 1/N)$. Accordingly, we define the desired codebook coherence by this value (i.e., $\mu_\theta^* = F(1/N)$), it then determines the codebook parameter β via an inverse mapping as $\beta = M(\mu_\theta^*)$.

2) Ring sampling: The rings are constructed to make the intra-ring coherence μ_θ resemble the FF case with $\Delta_R = 0$, which is computed between two points on the same ring. In contrast, the inter-ring coherence is evaluated for two points that lie on the same angular ray but belong to two different rings. For a given angle $\hat{\theta}_i$, those grid points are sampled as

$$\hat{r}_{i,s} = \frac{R_E(\hat{\theta}_i)}{4(s-1)\beta^2 + 1}, \quad s = 1, \cdots, S_i, \tag{12}$$

$$\Delta_r(\hat{\theta}_i) \triangleq \left| \frac{1}{\hat{r}_{i,s+1}} - \frac{1}{\hat{r}_{i,s}} \right| = \frac{4\beta^2}{R_E(\hat{\theta}_i)}, \tag{13}$$

where s indexes the points along $\hat{\theta}_i$ and stops increasing until entering the reactive NF region [1], [10] (i.e., $\hat{r}_{i,S_i+1} < R_F \triangleq 0.5\sqrt[3]{(Nd)^3/\lambda_c}$). The outermost ring corresponds to the ERD ring, whereas $r_{i,1} = R_E(\hat{\theta}_i) \triangleq 2N^2 d^2/\lambda_c(1-\hat{\theta}_i^2)$. Thus, the parameter β governs the sampling plan through the distance step $\Delta_r(\hat{\theta}_i)$ between two adjacent points $(\hat{r}_{i,s+1}; \hat{r}_{i,s})$.

Adopting the approximation on Fresnel functions in [4] for inter-ring coherence, we obtain the forward mapping as

$$\mu(\mathbf{W}) \approx \mu_\beta = G(\beta) = \tfrac{1}{\beta}\sqrt{C(\beta)^2 + S(\beta)^2}, \tag{14}$$

$$\beta = \tfrac{1}{2}\sqrt{R_E(\hat{\theta}_i) \cdot \Delta_r(\hat{\theta}_i)}, \tag{15}$$

where $C(\beta) = \int_0^\beta \cos\left(\frac{\pi}{2}t^2\right)dt, S(\beta) = \int_0^\beta \sin\left(\frac{\pi}{2}t^2\right)dt$ are the Fresnel integrals. As shown in the plot of $G(\beta)$ in Fig. 2b, a larger β may favor lower coherence, but it also increases the step distance Δ_r, reducing grid granularity with lower ring density. Particularly for $\beta > 1.6$, the distance ratio of the first two rings $\hat{r}_{i,1}/\hat{r}_{i,2} = 4\beta^2 + 1 > 11.24$, imposes an extreme large spacing between them (i.e., if $\hat{r}_{i,1} = 98.3$ m, then limiting $\hat{r}_{i,2} < 8.74$ m), leading to performance degradation due to an overly sparse grid accounting for a vast area in NF region.

In this work, we focus on the range $\beta \in [0, 1.6]$, then the inter-ring coherence μ_β should be in range of $[0.5, 1]$ accordingly. In addition, we also develop an inverse mapping for $\beta = G^{-1}(\mu) \approx M(\mu)$ by a polynomial of μ. Expanding the Fresnel integrals with a second-order Taylor series and applying several transformations, we derive the following

$$M(\mu) = \sqrt[4]{\tfrac{90(1-\mu)}{\pi^2}}\left[1 + \tfrac{5}{56}(1-\mu) + \tfrac{32}{6272}(1-\mu)^2\right]. \tag{16}$$

Higher-order terms of $(1-\mu)^k$ will shrink rapidly when k increases, especially with $\mu \in [0.5, 1]$. To sum up, our design can be summarized by the following chain, where ζ is chosen manually to employ the angular sampling by $I = \zeta \cdot N$,

$$\zeta^* \xrightarrow[2/(\zeta N)]{(10)} \Delta_\theta^* \xrightarrow[F(\Delta_\theta)]{(11)} \mu_\theta^* \xrightarrow[M(\mu_\theta)]{(16)} \beta^* \xrightarrow[\{(\hat{\theta}_i, \hat{r}_{i,s})\}]{(7),(10),(12)} \mathbf{W}. \tag{17}$$

Particularly, our codebook is constructed by $\zeta^* = 2$, which yields $(\mu_\theta^*, \beta^*) = (0.636, 1.39)$, as illustrated in Fig. 2.

B. Proposed unfolded model: Hybrid LISTA

Leveraging the iterative structure in (9) and integrating with the learning framework, the unfolding architecture can be reformulated for the computation at the t-th layer as

$$[\boldsymbol{\alpha}]^t = \mathcal{S}_{\theta^{(t)}}\left\{\mathbf{D}_1^{(t)}\mathbf{y} + \mathbf{D}_2^{(t)}[\boldsymbol{\alpha}]^{t-1}\right\}, \tag{18}$$

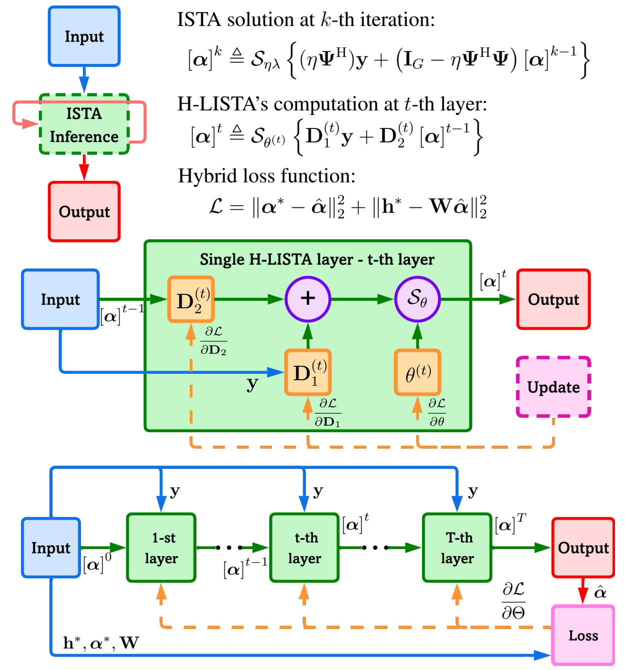

Fig. 3. The block diagram of Hybrid LISTA.

where T is the number of cascade ISTA layers, the set of learning parameters is denoted by $\Theta = \{\mathbf{D}_1^{(t)}, \mathbf{D}_2^{(t)}, \theta^{(t)}\}_{t=1}^T$. With the initial $[\boldsymbol{\alpha}]^{(0)} = \mathbf{0}$, these parameters are initialized identically for all ISTA layers as in (19), and they are untied to receive different gradient updates via back-propagation,

$$\mathbf{D}_1^{(0)} = \eta\boldsymbol{\Psi}^{\mathrm{H}}, \quad \mathbf{D}_2^{(0)} = \mathbf{I}_G - \eta\boldsymbol{\Psi}^{\mathrm{H}}\boldsymbol{\Psi}, \quad \theta^{(0)} = \eta\lambda. \tag{19}$$

The proposed loss function comprises contributions from both the estimated channel and its corresponding sparse representation. With the output from the last layer (i.e., $\hat{\boldsymbol{\alpha}} = [\boldsymbol{\alpha}]^T$), the hybrid loss function can be formally expressed as

$$\mathcal{L} = \gamma\, L_2(\hat{\boldsymbol{\alpha}}, \boldsymbol{\alpha}^*) + (1-\gamma)\, L_2(\mathbf{W}\hat{\boldsymbol{\alpha}}, \mathbf{h}^*) \tag{20}$$

$$= \gamma\, \|\boldsymbol{\alpha}^* - \hat{\boldsymbol{\alpha}}\|_2^2 + (1-\gamma)\, \|\mathbf{h}^* - \mathbf{W}\hat{\boldsymbol{\alpha}}\|_2^2, \tag{21}$$

where the given training labels are denoted by $\{\mathbf{h}^*, \boldsymbol{\alpha}^*\}$, with $\mathbf{h}^*$ is generated following (3) and its sparse representation $\boldsymbol{\alpha}^*$ corresponds to codebook $\mathbf{W}$ in (7). The structure of our proposed H-LISTA can be depicted as in Fig. 3.

IV. Simulation Results

In this section, we present numerical experiments to evaluate the behavior of our designed codebook and the performance of the proposed deep unfolded network H-LISTA for NF channel estimation.

A. Simulation Configuration

We consider an ELAA system equipped with $N = 256$ antennas at the BS, operating at $f_c = 100$ GHz and serving $K = 4$ users simultaneously. Under these parameters, the NF boundary extends to 98.3 m. The BS employs a hybrid precoding architecture with $N_{\mathrm{RF}} = 4$ RF chains and $P = 32$ pilot symbols, resulting in a compression ratio of

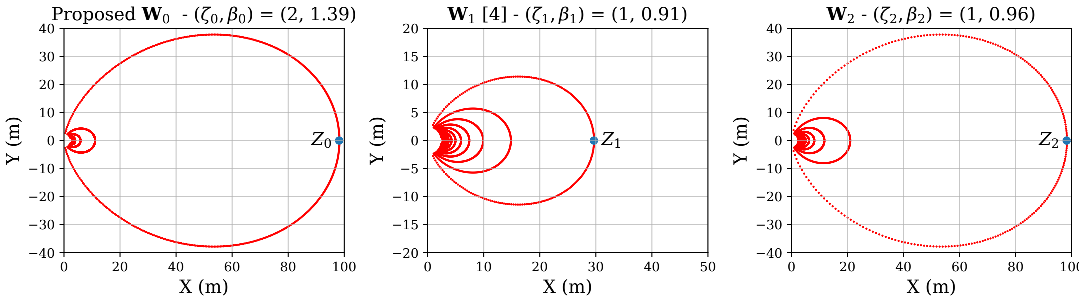

Fig. 4. Illustration of compared codebook grids in 2D spatial space.

$P \cdot N_{\mathrm{RF}}/N = 0.5$ for matrix $\mathbf{A}$. The Lagrange multiplier in (P_1) is set to $\lambda = 0.5$.

The NF channel $\mathbf{h}^*$ is generated according to (3) with $L = 6$ paths. For each path, the complex gain is drawn as $g_l \sim \mathcal{CN}(0, 1)$, while the distance r_l and angle θ_l are uniformly sampled from $\mathcal{U}(15, 95)$ m and $\mathcal{U}(-\sqrt{3}/2, \sqrt{3}/2)$, respectively. The estimation performance of $\hat{\mathbf{h}}$ is quantified by the normalized mean squared error (NMSE) as

$$\mathrm{NMSE\ (dB)} = 10 \log_{10} \mathbb{E} \left\{ \frac{\|\mathbf{h}^* - \mathbf{W}\hat{\boldsymbol{\alpha}}\|_2^2}{\|\mathbf{h}^*\|_2^2} \right\}. \tag{22}$$

For training, we employ training and validation datasets comprising 20480 and 5120 samples, respectively. They are generated with the SNR of the received signals uniformly over a range of $[0, 30]$ dB, where the validation set is used for early stopping. The test sets are generated at specific SNR values $\{0, 5, 10, \ldots, 25, 30\}$ dB, each containing 1024 samples. The proposed model is trained using the `Adam` optimizer with a learning rate of 10^{-4}, each batch containing 512 samples, and the hybrid loss hyperparameter is set to $\gamma = 0.5$.

B. Experimental Results

Fig. 4 and Fig. 5 provide the illustration and evaluation for our proposed codebook $\mathbf{W}_0$ against two other codebooks $\mathbf{W}_1$ [4] and its extension $\mathbf{W}_2$ with the inclusion of an ERD ring. To ensure a fair comparison, all three codebooks are built with a comparable number of grid points, yet those codebooks still exhibit higher mutual coherence than our proposed one. Their detailed configurations are summarized in Table I. The inclusion of the outermost ring enables $\mathbf{W}_2$ to achieve better estimation accuracy than the original $\mathbf{W}_1$, confirming the necessity of codebook coverage in the NF region with outer ring distances $Z_1 = 29.68$ m and $Z_2 = 98.3$ m, respectively. By trading off the granularity of the grid for enhanced angular sampling, $\mathbf{W}_0$ employs much fewer rings in the spatial domain. As illustrated in Fig. 5, $\mathbf{W}_0$ consistently outperforms both $\mathbf{W}_1$ and $\mathbf{W}_2$ across all SNR levels. This emphasizes that finer angular resolution significantly enhances performance and should be prioritized over increasing ring density. Overall, with a similar number of grid points, $\mathbf{W}_0$ effectively covers the NF region while maintaining relatively low mutual coherence, and still delivers superior estimation performance compared to the other codebooks.

To verify the performance behavior of our proposed H-LISTA in terms of computational efficiency and estimated

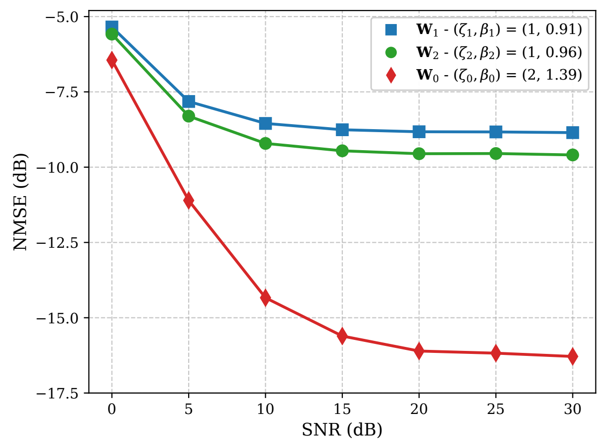

Fig. 5. Performance evaluation of compared codebooks.

TABLE I
CODEBOOK'S PARAMETER CONFIGURATION.

Parameter's Descriptions		$\mathbf{W}_0$	$\mathbf{W}_1$	$\mathbf{W}_2$
Coherence parameter	β	1.39	0.91	0.96
Increased angular density	ζ	2	1	1
Number of sampled points	G	**1874**	1890	1886
Codebook coherence	μ	**0.64**	0.93	0.91
Outermost ring distance	Z	**98.3**	29.68	98.3

performance, we experiment with randomized SNR levels, as shown in Fig. 6. Each layer of the unfolded model corresponds to one iteration of the conventional iterative solvers [14]. Although FISTA converges much faster than standard ISTA due to its momentum-based acceleration, both still suffer from slow convergence relative to unfolded models. In this experiment, we also perform two other deep unfolding-based models: LISTA [8] and LISTA-CP [9]. Both are trained with a loss function solely based on sparse representation as $L_2(\hat{\boldsymbol{\alpha}}, \boldsymbol{\alpha}^*)$, where LISTA-CP is built upon a LISTA variant [14] that coupling $\mathbf{D}_2^{(t)} = \mathbf{I} - \mathbf{D}_1^{(t)}\boldsymbol{\Psi}$, thereby reducing its learnable parameters $\Theta_{\mathrm{CP}} = \{\mathbf{D}_1^{(t)}, \theta^{(t)}\}_{t=1}^{T}$. Remarkably, with only two layers, our proposed model still achieves estimation performance comparable to LISTA and LISTA-CP, both of which employ ten layers. Among the unfolded models, LISTA-CP is the slowest one, this occurs due to its limited learnable parameter set, and the coupling weight mechanism in [14] requires a strict low-coherence condition. Moreover, stacking more intermediate layers (i.e., more than six layers), both LISTA and our H-LISTA yield no significant improvements

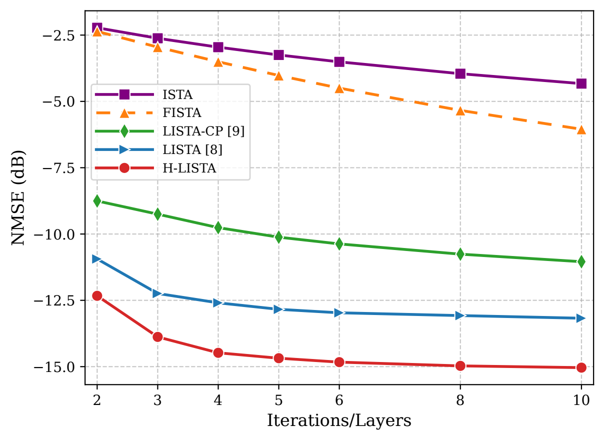

Fig. 6. Performance of different configurations under randomized SNR.

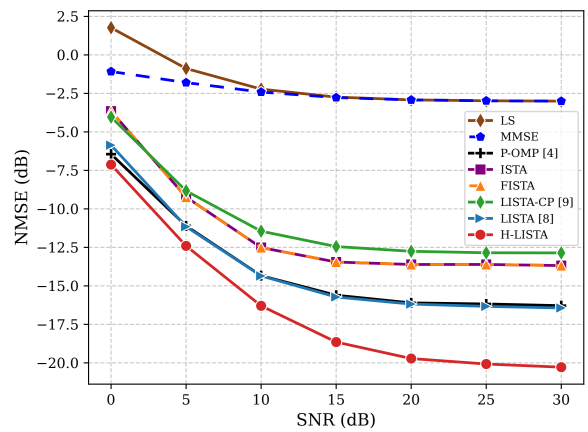

Fig. 7. Performance of estimation schemes with the varying SNR.

in estimation performance. Therefore, the H-LISTA model composed of six layers, is our preferred configuration to balance reconstruction error and the number of parameters, since more layers would require optimizing more parameters.

To evaluate the performance of our proposed channel estimation scheme, we compare it with several existing approaches under varying SNR levels, as shown in Fig. 7. Conventional direct estimators, such as least squares (LS) and minimum mean square error (MMSE), yield only poor estimation accuracy due to the wide shape of the measurement matrix $\mathbf{A}$ and their disregard for channel sparsity. By exploiting the sparse representation in the polar domain, CS-based methods such as polar-domain orthogonal matching pursuit (P-OMP) [4] and the iterative algorithms ISTA and FISTA achieve significantly better estimation performance. Among conventional CS approaches, P-OMP achieves the best accuracy, but it requires a sparsity level as a stopping criterion, which is typically chosen heuristically through simulations as in [4]. In contrast, ISTA and FISTA dynamically solve the optimization problem in (P_1), but they both suffer from slow convergence: ISTA and FISTA take roughly 1000 and 200 iterations, respectively. By leveraging an additional channel reconstruction error term $L_2(\mathbf{W}\hat{\boldsymbol{\alpha}}, \mathbf{h}^*)$, our proposed H-LISTA, which employs only six layers, consistently outperforms all other unfolded models across the entire SNR range.

V. Conclusions

This work has investigated NF channel estimation in ELAA systems by leveraging the sparsity of channels in the polar domain. We have proposed a codebook design guideline that deliberately controls the mutual coherence through the sampling strategy. We also developed a deep unfolding network, termed Hybrid LISTA, with a mixed loss function that incorporates both the target channel and its sparse representation. Numerical results demonstrate that our proposed codebook efficiently covers the entire NF region while achieving lower estimation error. Moreover, with the additional channel information embedded in the loss function, our unfolded model consistently outperforms existing channel estimation schemes across a wide range of SNR levels, while using significantly fewer intermediate layers than other deep unfolded networks. For future work, one may extend this framework to MIMO system where users are also equipped with antenna arrays.

References

[1] Y. Liu, Z. Wang, J. Xu, C. Ouyang, X. Mu, and R. Schober, "Near-field communications: A tutorial review," *IEEE Open J. Commun. Soc.*, vol. 4, pp. 1999–2049, 2023.

[2] S. Ye, M. Xiao, M.-W. Kwan, Z. Ma, Y. Huang, G. Karagiannidis, and P. Fan, "Extremely large aperture array (ELAA) communications: Foundations, research advances and challenges," *IEEE Open J. Commun. Soc.*, vol. 5, pp. 7075–7120, 2024.

[3] E. J. Candes, Y. C. Eldar, D. Needell, and P. Randall, "Compressed sensing with coherent and redundant dictionaries," *Appl. Comput. Harmon. Anal.*, vol. 31, no. 1, pp. 59–73, 2011.

[4] M. Cui and L. Dai, "Channel estimation for extremely large-scale MIMO: Far-field or near-field?" *IEEE Trans. Commun.*, vol. 70, no. 4, pp. 2663–2677, 2022.

[5] X. Zhang, H. Zhang, and Y. C. Eldar, "Near-field sparse channel representation and estimation in 6G wireless communications," *IEEE Trans. Commun.*, vol. 72, no. 1, pp. 450–464, 2024.

[6] N. Shlezinger and Y. C. Eldar, "Model-based deep learning," *Found. Trends Signal Process.*, vol. 17, no. 4, pp. 291–416, 2023.

[7] K. Gregor and Y. LeCun, "Learning fast approximations of sparse coding," in *Int. Conf. Int. Conf. Mach. Learn. (ICML)*, 2010, p. 399–406.

[8] X. Zhang, Z. Wang, H. Zhang, and L. Yang, "Near-field channel estimation for extremely large-scale array communications: A model-based deep learning approach," *IEEE Commun. Lett.*, vol. 27, no. 4, pp. 1155–1159, 2023.

[9] J. Yang, B. Ai, W. Chen, S. Yang, G. Shi, N. Wang, and C. Yuen, "Deep learning-based near-field wideband channel estimation: A joint LISTA-CP approach," *IEEE Trans. Veh. Technol.*, vol. 74, no. 9, pp. 14 041–14 053, 2025.

[10] N. T. Khang, D. H. Son, T. T. Duy, T. T. Le, T. T. T. Quynh, K. Abed-Meraim, M. Debbah, and N. L. Trung, "Ray-tracing channel models for near-field communication," *VNU J. Sci.: Comput. Sci. Commun. Eng.*, vol. 42, no. 3, 2026.

[11] A. Bruckstein, D. Donoho, and M. Elad, "From sparse solutions of systems of equations to sparse modeling of signals and images," *SIAM Rev.*, vol. 51, pp. 34–81, 2009.

[12] I. Daubechies, M. Defrise, and C. De Mol, "An iterative thresholding algorithm for linear inverse problems with a sparsity constraint," *Commun. Pure Appl. Math.*, vol. 57, no. 11, pp. 1413–1457, 2004.

[13] M. Cui and L. Dai, "Near-field wideband channel estimation for extremely large-scale MIMO," *Sci. China Inf. Sci.*, vol. 66, no. 7, p. 172303, 2023.

[14] X. Chen, J. Liu, Z. Wang, and W. Yin, "Theoretical linear convergence of unfolded ISTA and its practical weights and thresholds," in *Adv. Neural Inf. Process. Syst. (NeurIPS)*, 2018, p. 9079–9089.